Influence of surface structures, subsurface carbon and hydrogen, and surface alloying on the activity and selectivity of acetylene hydrogenation on Pd surfaces: A density functional theory study

Yang, B., Burch, R., Hardacre, C., Headdock, G., & Hu, P. (2013). Influence of surface structures, subsurface carbon and hydrogen, and surface alloying on the activity and selectivity of acetylene hydrogenation on Pd surfaces: A density functional theory study. *Journal of Catalysis*, *305*, 264-276. https://doi.org/10.1016/j.jcat.2013.05.027

Published in:
Journal of Catalysis

Document Version:
Publisher's PDF, also known as Version of record

Queen's University Belfast - Research Portal:
Link to publication record in Queen's University Belfast Research Portal

Journal of Catalysis 305 (2013) 264–276

Contents lists available at SciVerse ScienceDirect

Journal of Catalysis

journal homepage: www.elsevier.com/locate/jcat

Influence of surface structures, subsurface carbon and hydrogen, and surface alloying on the activity and selectivity of acetylene hydrogenation on Pd surfaces: A density functional theory study ☆

Bo Yang [a], Robbie Burch [a], Christopher Hardacre [a,*], Gareth Headdock [b], P. Hu [a,*]

[a] CenTACat, School of Chemistry & Chemical Engineering, Queen's University Belfast, Belfast BT9 5AG, UK
[b] Johnson Matthey Catalysts, PO Box 1, Billingham, Teesside TS23 1LB, UK

ARTICLE INFO

Article history:
Received 1 February 2013
Revised 12 May 2013
Accepted 26 May 2013
Available online 28 June 2013

Keywords:
DFT
Acetylene hydrogenation
Activity
Selectivity
Two-step model
Subsurface carbon and hydrogen
Surface alloy
Energy decomposition

ABSTRACT

The selective hydrogenation of acetylene to ethylene on several Pd surfaces (Pd(1 1 1), Pd(1 0 0), Pd(2 1 1), and Pd(2 1 1)-defect) and Pd surfaces with subsurface species (carbon and hydrogen) as well as a number of Pd-based alloys (Pd–M/Pd(1 1 1) and Pd–M/Pd(2 1 1) (M = Cu, Ag and Au)) are investigated using density functional theory calculations to understand both the acetylene hydrogenation activity and the selectivity of ethylene formation. All the hydrogenation barriers are calculated, and the reaction rates on these surfaces are obtained using a two-step model. Pd(2 1 1) is found to have the highest activity for acetylene hydrogenation while Pd(1 0 0) gives rise to the lowest activity. In addition, more open surfaces result in over-hydrogenation to form ethane, while the close-packed surface (Pd(1 1 1)) is the most selective. However, we also find that the presence of subsurface carbon and hydrogen significantly changes the reactivity and selectivity of acetylene toward hydrogenation on Pd surfaces. On forming surface alloys of Pd with Cu, Ag and Au, the selectivity for ethylene is also found to be changed. A new energy decomposition method is used to quantitatively analyze the factors in determining the changes in selectivity. These surface modifiers are found to block low coordination unselective sites, leading to a decreased ethane production.

1. Introduction

The selective hydrogenation of acetylene in excess ethylene is an industrially important process [1,2]. Ethylene is one of the most widely produced petrochemicals and is commonly made by the steam-mediated thermal cracking of higher hydrocarbons in high-temperature furnaces. However, the thermal processes also produce about 0.1–1% of acetylene and, importantly, acetylene poisons the downstream catalyst used for the polymerization of ethylene. Furthermore, the presence of acetylene also affects the quality of the poly-ethylene produced. The most widely used method to solve the problem is to selectively hydrogenate acetylene to ethylene using palladium-based heterogeneous catalysts. The objective is to hydrogenate acetylene to ethylene, leading to purification of ethylene and a higher ethylene yield.

The major concern in the acetylene removal processes consists of two issues, namely hydrogenation of ethylene to ethane and the formation of high molecular weight oligomeric species known as "green oil." The over-hydrogenation results in a loss of ethylene and reducing the effective reactant concentration for the subsequent polymerization, while green oil formation on the surface of the catalyst leads to the deactivation of the catalyst and also loss of hydrocarbon [3–5]. The challenge is to develop highly selective catalysts that have both low ethane production and green oil formation.

Extensive work has been undertaken, both experimentally and theoretically, to improve the performance of the widely used palladium catalyst by adding promoters such as metals, metal oxides, and modifiers such as CO [6] and N_2O [7,8]. Currently, the most commonly employed catalysts are based on supported Pd–Ag bimetallic systems [9–11]. Pd modified with Au [12], Cu [13], Ga [14–17], Pb [18], Zn [19], Ce [20], and K [21,22] have been used to improve the performance of the catalysts. Metal oxides such as CeO_2 [23], TiO_2 [24,25], Nb_2O_5 [26], and SiO_2 [27] have also been studied experimentally. In the search for non-precious metallic catalysts, Nørskov and co-workers used density functional theory (DFT) calculations to optimize the metal combinations and developed a highly selective Ni–Zn bimetallic catalyst that prevents over-hydrogenation [28]. More recently, Bridier and Pérez-Ramírez reported a ternary Cu–Ni–Fe catalyst with a relatively high

* Corresponding authors. Fax: +44 2890 974687 (C. Hardacre).
E-mail addresses: c.hardacre@qub.ac.uk (C. Hardacre), p.hu@qub.ac.uk (P. Hu).

0021-9517/$ - see front matter © 2013 The Authors. Published by Elsevier Inc. All rights reserved.
http://dx.doi.org/10.1016/j.jcat.2013.05.027

selectivity to alkenes; however, in this case, significantly higher operating temperatures were needed compared with those used with the palladium-based systems [29]. Moreover, Ni–Al mixed oxides based on a hydrotalcite-type structure were also found to have a good selectivity for the hydrogenation of acetylene to ethylene [30]. In addition to promoters, the catalyst has been found to change during reaction with the formation of subsurface species like C and H. These are thought to have some effect on the selectivity of acetylene hydrogenation to ethylene [31–34].

Although acetylene hydrogenation reactions have been studied theoretically on both pure Pd and bimetallic Pd–Ag surfaces [35–40], the crucial role of the surface structures as well as the interplay between the surface structure and the presence of subsurface carbon and hydrogen species, since the formation of carbide or hydride during the hydrogenation may occur during the reaction of acetylene hydrogenation on Pd [31,32,41–44], and the effect of alloying on the activities and selectivity have yet to be described in detail. Therefore, in the current work, a number of surfaces have been studied, which are summarized below:

1. Flat (Pd(111) and Pd(100)) and stepped (Pd(211)) surfaces in order to examine the activity and selectivity for acetylene hydrogenation using DFT calculations. In addition, a defective Pd(211) surface containing lower coordinated Pd atoms than that on a standard Pd(211) surface has also been examined.
2. The effect of the presence of subsurface carbon and hydrogen species on the activity and selectivity of acetylene hydrogenation on Pd(111) and Pd(211).
3. The alloying effects of surface Cu, Ag, and Au on Pd(111) and Pd(211) and only the effects of them regarding the selectivity of ethylene formation are considered.

2. Computational details

DFT calculations were performed with the Vienna Ab-initio Simulation Package (VASP) in slab models [45–48]. The exchange-correlation functional PW91 was used to calculate the electronic structure with generalized gradient approximation (GGA) [49]. The projector augmented wave (PAW) method was employed to describe the interaction between the atomic cores and electrons [50,51]. For Pd(111), Pd(100) and those Pd(111) with subsurface species, surface alloys on Pd(111), four layer 2×2 unit cells with the top two layers relaxed during optimization were used to model the adsorption and reaction processes. Each surface alloy was modeled with the different coverage patterns was modeled with the substitution of surface Pd atoms with Cu, Ag, and Au atoms. A $5 \times 5 \times 1$ *k*-point sampling in the surface Brillouin zone was used for the Pd(111), Pd(111)–C, Pd(111)–H, and Pd–M/Pd(111) (M = Cu, Ag, and Au) surfaces while the *k*-point sampling used for Pd(100) was $3 \times 3 \times 1$. For Pd(211), defective Pd(211) and Pd(211) with subsurface species, surface alloys associated with Pd(211), 12 atomic layers with 1×2 surface supercells were employed with a $4 \times 2 \times 1$ *k*-point grid and the top 6 layers were relaxed together with the surface adsorbates. The defective Pd(211) surface, which is denoted as Pd(211)-defect, hereafter, was modeled by removing two Pd atoms at the step site thus forming two low-coordinated Pd atoms at the step site, as shown in the Supporting information. The surface alloys of Pd–M/Pd(211) (M = Cu, Ag, and Au) were modeled with the substitution of a whole row of Pd atoms at the step edge site with Cu, Ag, and Au. The vacuum was set to be more than 12 Å. A cutoff energy of 500 eV and the converging criteria of the force on each relaxed atoms below 0.05 eV $Å^{-1}$ were used in this work. The transition states were located with a constrained minimization method [52–54]. The adsorption energies are defined as:

$$E_{ad} = E_{total} - (E_g + E_{slab}) \quad (1)$$

where E_{total} is the energy of the system after adsorption, E_g is the energy of the gas-phase molecule, and E_{slab} is the energy of the slab.

López and co-workers recently studied the stability of Pd surfaces alloyed with Cu, Ag, and Au atoms [55]. They found that the solubility, near surface alloy formation, and islands formation of these metals on Pd surface were less favorable than other metals investigated. Therefore, in this paper, the Cu-, Ag-, and Au-doped Pd catalysts were modeled as surface alloys.

The free energies of gas-phase species were calculated using the equation $G = H - TS$. The entropic effect was only considered for the adsorption and desorption processes while the surface reaction energetics were estimated by the total energy ones. The temperature was set to 350 K, which lies in the range of the temperatures used under the industrial conditions (313–373 K). The total pressure was set to 10 atm and the partial pressures of C_2H_2, H_2, and C_2H_4 are 0.1 atm, 1 atm, and 8.9 atm, respectively, which are very similar to the experimental conditions. The entropies of C_2H_2, H_2, and C_2H_4 under standard conditions used in this paper were obtained from experimental databases [56,57]. The system studied herein is based on the front-end process wherein the H_2/C_2H_2 ratio is high and the selectivity to ethylene is the major problem. Therefore, the oligomerization of acetylene on the catalyst surface was not considered in the current work.

3. Results and discussion

3.1. Influence of surface structures on the activity and selectivity of ethylene formation on Pd

3.1.1. Ethylene formation from acetylene hydrogenation on flat and stepped surfaces of Pd

The adsorption energies for the reactant C_2H_2 and the product C_2H_4 and their adsorption geometries together with the adsorption geometries of the intermediate C_2H_3 on Pd(111), Pd(100), Pd(211), and Pd(211)-defect surfaces are shown in Table 1 and Fig. 1, respectively. On Pd(111), the adsorption geometries of these species are consistent with previous results, showing that the favorable adsorption of C_2H_2 and C_2H_3 occurs at the 3-fold hollow sites while C_2H_4 is bound in a di-σ configuration [34,35,58–66]. Similarly, hollow sites are preferred for the adsorption of both C_2H_2 and C_2H_3 on Pd(100). In this case, both C_2H_2 and C_2H_3 bind to four Pd atoms and the adsorption energy of C_2H_2 on Pd(100) is found to be much higher than that found on Pd(111). The adsorption geometry of C_2H_4 at Pd(100) is the same as that found on Pd(111), which shows a di-σ configuration. Again, the adsorption is stronger on the (100) surface compared with the (111) surface.

Comparing the step and corner sites, i.e., Pd(211) and Pd(211)-defect surfaces, respectively, shows that both the adsorption geometries and energies of C_2H_2 on each site are similar. The C_2H_2 was found to adsorb on the 4-fold site under the step edge (B5 site), whereas the C_2H_4 was found to adsorb on the step edge with a di-σ configuration, which is consistent with previously reported results [67]. The adsorption energy of C_2H_2 on Pd(211) is 0.1 eV lower than that on Pd(211)-defect site, but the adsorption energy of C_2H_4 on Pd(211) is only 0.01 eV higher than that on

Table 1
Adsorption energies (eV) of acetylene and ethylene on Pd(111), Pd(100), Pd(211), and Pd(211)-defect surfaces, which are calculated from Eq. (1).

	Pd(111)	Pd(100)	Pd(211)	Pd(211)-defect
C_2H_2	−1.94	−2.66	−2.26	−2.36
C_2H_4	−0.85	−0.96	−1.17	−1.16

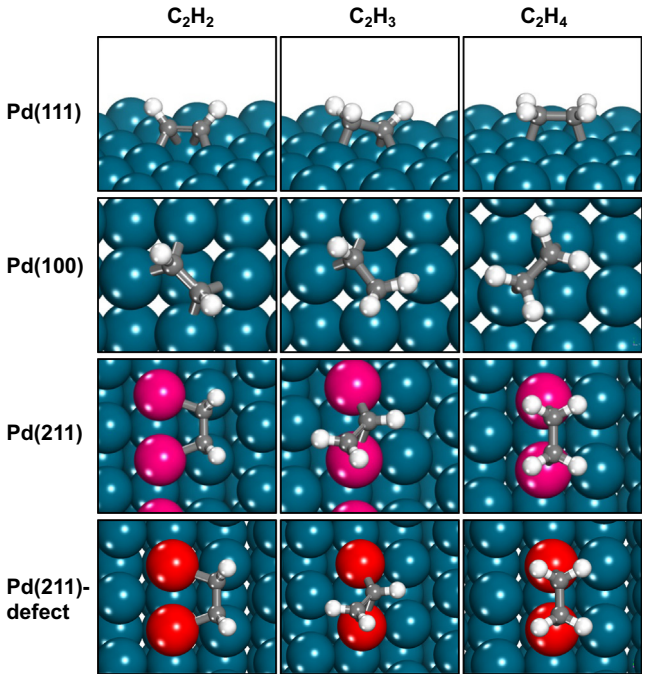

Fig. 1. Adsorption structures of C_2H_2, C_2H_3, and C_2H_4 on Pd(111), Pd(100), Pd(211), and Pd(211)-defect surfaces. Those low-coordinated Pd atoms of Pd(211) and Pd(211)-defect surfaces are shown in red. The gray and white balls denote carbon and hydrogen atoms, respectively. This notation is used throughout this paper. (For interpretation of the references to color in this figure legend, the reader is referred to the web version of this article.)

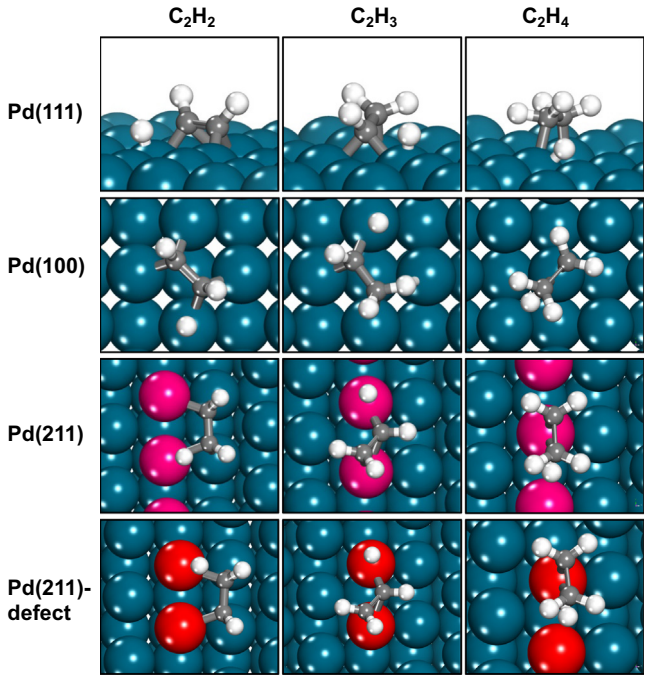

Fig. 2. Transition-state structures of C_2H_2, C_2H_3, and C_2H_4 hydrogenation on Pd(111), Pd(100), Pd(211), and Pd(211)-defect surfaces. Those low-coordinated Pd atoms of Pd(211) and Pd(211)-defect surfaces are shown in red. (For interpretation of the references to color in this figure legend, the reader is referred to the web version of this article.)

Pd(211)-defect surface, which is within the uncertainty associated with DFT calculations.

The hydrogenation barriers of C_2H_2 and C_2H_3 and the C–H distances at the TSs on Pd(111), Pd(100), Pd(211), and Pd(211)-defect surfaces are listed in Table 2, and Fig. 2 shows the geometries of these transition states. The hydrogenation barriers of C_2H_2 on all the surfaces studied were found to be similar; however, those of C_2H_3 were much higher on the Pd(111) and Pd(100) surfaces compared with the Pd(211) and Pd(211)-defect surfaces.

The energy profiles of acetylene hydrogenation to produce ethylene on all the surfaces are shown in Fig. 3, in which the entropic effects are considered for the adsorption and desorption processes. It should be noted that both C_2H_2 and H_2 must adsorb on the catalyst surface and, therefore, their relative adsorption barriers should be compared in order to obtain the rate-determining process.

Our previous work investigated the barriers of the adsorption and desorption processes in heterogeneous catalysis with three methods, namely immobile, mobile, and collision theory [68]. The detailed methodology to obtain the adsorption barriers is reported in the Supporting information and the references given. It was found that the transition-state energy of the adsorption process was always lower than the gaseous total energy of the species, and thus, the TS_R of species R (R = C_2H_2 or H_2) can be considered to be the maximum adsorption barrier of R, where T is the reaction temperature and S_R is the entropy of the species R at the temperature T [68]. In the current work, the TS of C_2H_2 and H_2 is calculated to be 0.72 eV and 0.47 eV at 350 K, respectively, indicating that the adsorption of C_2H_2 has the higher adsorption barrier. Therefore, the adsorption barrier of C_2H_2 (0.72 eV) can be considered as the limiting adsorption barrier of the reactants. However, we will show below that the choice of the adsorption barrier will not influence our conclusions.

Table 2
Reaction barriers (E_a) and C–H distances at the TSs of the whole pathway of acetylene hydrogenation to C_2H_4 on Pd(111), Pd(100), Pd(211), and Pd(211)-defect surfaces.

	C_2H_2 + H		C_2H_3 + H	
	E_a (eV)	Distance (Å)	E_a (eV)	Distance (Å)
Pd(111)	0.96	1.67	0.89	1.76
Pd(100)	0.93	1.64	0.74	1.72
Pd(211)	0.97	1.64	0.55	1.75
Pd(211)-defect	1.08	1.67	0.56	1.83

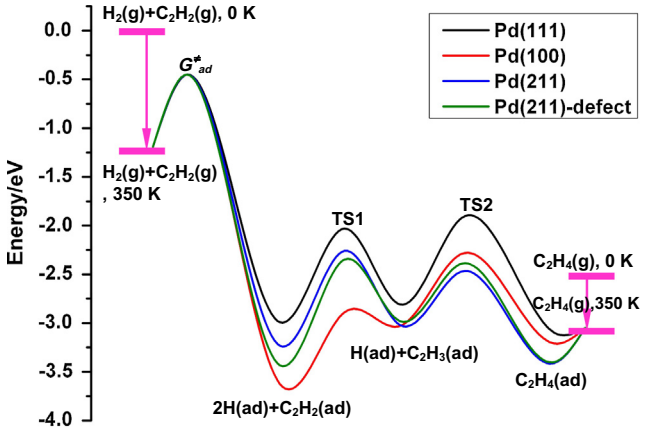

Fig. 3. Energy profiles of C_2H_2 hydrogenation on Pd(111), Pd(100), Pd(211), and Pd(211)-defect surfaces under the standard pressure; the entropy effect is considered for the adsorption and desorption processes here. $G^{\neq}_{ad}$ is the transition-state energy of the adsorption of C_2H_2 on all the surfaces.

3.1.2. Selectivity of ethylene formation on flat and stepped surfaces

The hydrogenation of C_2H_4 over a range of Pd surfaces was investigated in order to understand their influence on the

selectivity of ethylene formation. Table 3 summarizes the hydrogenation barriers of ethylene and the C–H distances at the TSs on all the surfaces studied. Although the most stable adsorption configuration of ethylene on all the Pd surfaces is found to be the di-σ, the transition-state energies for the hydrogenation of ethylene from both di-σ and π configurations were calculated. The hydrogenation barriers listed in Table 3 are those lower values for each surface. The hydrogenation barrier was found to be the lowest at Pd(100) with a value of 0.66 eV while it is highest on the Pd(111) with a value of 0.91 eV. Moreover, the hydrogenation of those π-bonded ethylene on Pd(100), Pd(211), Pd(211)-def are favored, while the hydrogenation of di-σ-bonded ethylene is only favored over Pd(111). In addition to the hydrogenation barrier of ethylene, the desorption barrier of ethylene will also affect the selectivity as this determines the surface concentration of ethylene [28]. The simplest way to compare the selectivity on different surfaces is to examine the difference between ethylene desorption and hydrogenation barriers on these surfaces, which has been widely used by other groups [28,32,35,38]. The most selective catalyst should have a low desorption barrier with a relatively high hydrogenation barrier, as reported by Nørskov et al. [28]. However, the desorption barrier is not easy to be calculated *vide supra*.

From previous studies by our group [68], the desorption barrier was always found to be slightly lower than the absolute value of adsorption energy. Nevertheless, as the difference between them is relatively small, the desorption barrier is considered approximately to equal the absolute value of adsorption energy, which was also used in our previous study [69–71]. Therefore, in this study the difference between the hydrogenation barrier for C_2H_4 and the absolute value of C_2H_4 adsorption energy, which is denoted as ΔE_a in Eq. (2), was used to compare the selectivities:

$$\Delta E_a = E_{a,hydr} - E_{a,des} = E_{a,hydr} - |E_{ad}| \tag{2}$$

The variation of ΔE_a on Pd(111), Pd(211) and Pd(211)-defect is shown in Table 3. ΔE_a is found to be positive on Pd(111) whereas on all other surfaces it is negative, indicating that the desorption of C_2H_4 is strongly favored over Pd(111) compared with Pd(100), Pd(211) and Pd(211)-defect surfaces. This suggests that the relatively low selectivity of C_2H_4 in C_2H_2 hydrogenation over pure Pd catalysts is probably caused by favorable C_2H_4 adsorption and the subsequent over-hydrogenation at low coordination sites.

The hydrogenation of C_2H_3 ($CHCH_2$) at both carbons was calculated forming $CHCH_3$ and CH_2CH_2. This is important as there are some results reporting that the formation of $CHCH_3$ will also influence the selectivity of ethylene formation [34]. It was found that, on Pd(111), although the formation barriers of both products are the same (0.89 eV), the energy of the adsorption state of $CHCH_3$ and the transition state of its further hydrogenation are 0.31 eV and 0.30 eV higher than found for CH_2CH_2, respectively, indicating that the formation of C_2H_5 via the $CHCH_2 + 2H \rightarrow CHCH_3 + H \rightarrow CH_2CH_3$ pathway is much less favored than the pathway associated with $CHCH_2 + 2H \rightarrow CH_2CH_2 + H \rightarrow CH_2CH_3$. More importantly, the desorption of ethylene from the surface is favored over all the pathways studied on Pd(111). For more open faces, the hydrogenation barriers of $CHCH_2 + H \rightarrow CHCH_3$ were always found to be higher than found for $CHCH_2 + H \rightarrow CH_2CH_2$ and, therefore, the pathway via $CHCH_3$ was not considered further in the current work.

Table 3
Hydrogenation barriers (E_a) of ethylene and C–H distances at the TSs on the flat and step surfaces of Pd. The calculated values of ΔE_a, according to Eq. (2), are also listed.

	Pd(111)	Pd(100)	Pd(211)	Pd(211)-defect
E_a (eV)	0.91	0.66	0.72	0.78
Distance (Å)	1.52	1.42	1.43	1.43
ΔE_a (eV)	0.06	−0.30	−0.45	−0.38

3.1.3. General discussion on the activity on Pd surfaces

In our previous work, a two-step model was proposed to describe catalytic processes on solid surfaces which can be generalized as:

$$\begin{aligned} R_g + * &\rightleftharpoons I_{ad} \\ I_{ad} &\rightleftharpoons P_g + * \end{aligned} \tag{3}$$

where R_g and P_g are the gas-phase reactants and products, I_{ad} is the adsorption state of the intermediate species [72,73]. In the current work, the model has been applied to estimate the activity of acetylene hydrogenation. In this case, R_g is $C_2H_2 + H_2$ and P_g is C_2H_4. The energy profile of the two step model of acetylene hydrogenation is shown in Fig. 4.

The adsorption rate (r_{ad}) and desorption rate (r_{de}) can be written as

$$r_{ad} = \frac{k_B T}{h} e^{-\frac{E_R^{ad}}{RT}} \frac{P_R}{P^0} \theta_* (1 - z_{ad}) \tag{4}$$

$$r_{de} = \frac{k_B T}{h} e^{-\frac{E_P^{de}}{RT}} \theta_I (1 - z_{de}) \tag{5}$$

where P_R, P_P, and P^0 are the partial pressures of the reactants and the products and standard pressure, respectively. E_R^{ad} and E_P^{de} are the effective barriers of the reactant adsorption and the product desorption, respectively. z_{ad} and z_{de} are the reversibility of the adsorption and desorption, respectively, and can be written as

$$z_{ad} = \frac{P^0 \theta_I}{P_R \theta_* K_{ad}} \tag{6}$$

$$z_{de} = \frac{P_P \theta_*}{P^0 \theta_I K_{de}} \tag{7}$$

where K_{ad} and K_{de} is the equilibrium constant of the adsorption and desorption processes, relatively. Using the steady state condition, i.e., $r = r_{ad} = r_{de}$ and the coverage relationship $\theta_I + \theta_* = 1$, the reaction rate can be written:

$$r = \frac{k_B T}{h} \frac{\left(1 - \frac{P_P}{P_R} e^{\frac{\Delta G}{RT}}\right)}{\frac{P^0}{P_R} e^{\frac{E_R^{ad}}{RT}} + \frac{P^0}{P_R} e^{\frac{E_R^{ad} - E_R^{de} + E_P^{de}}{RT}} + e^{\frac{E_P^{de}}{RT}} + \frac{P_P}{P_R} e^{-\frac{\Delta G + E_R^{de}}{RT}}} \tag{8}$$

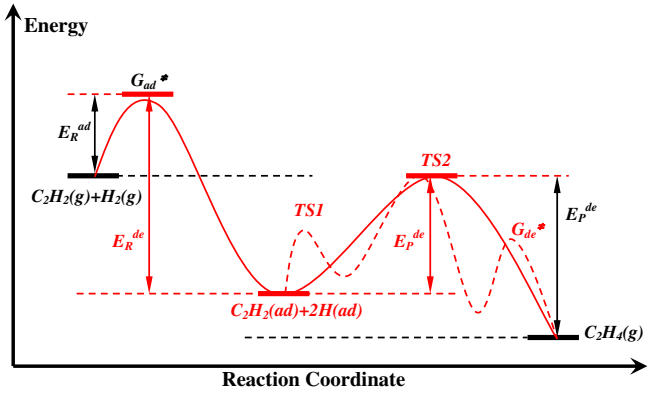

Fig. 4. Two-step model, namely the adsorption of the reactants ($C_2H_2 + H_2$) and associative desorption of the products (C_2H_4), of acetylene hydrogenation to form ethylene process. E_R^{ad} and E_R^{de} are the barriers of the adsorption of the reactants and its reverse reaction, respectively. Similarly, E_P^{ad} and E_P^{de} are the barriers of the adsorption of the products and its reverse reaction, respectively. TS1 and TS2 are the same as those shown in Fig. 3. $G_{ad}^{\neq}$ and $G_{de}^{\neq}$ is the transition state of the adsorption of the reactants and the desorption of the products, respectively.

ΔG is the free energy change of the overall reaction, E_P^{ad} and E_R^{de} are the adsorption barriers of the product and the desorption barrier of the reactant, respectively. The details of the derivation of Eq. (8) can be found in Ref. [72]. For the present system associated with acetylene hydrogenation on Pd surfaces, we can reasonably assume that the process is desorption rate limited. Therefore, the adsorption process reaches quasi-equilibrium, and thus z_{ad} is close to 1 and the reaction rate can be expressed as:

$$r = \frac{k_B T}{h} \frac{\left(1 - \frac{P_P}{P_R} e^{\frac{\Delta G}{RT}}\right)}{\frac{p^0}{P_R} e^{\frac{E_R^{ad} - E_R^{de} + E_P^{de}}{RT}} + e^{\frac{E_P^{de}}{RT}}} \quad (9)$$

Since the adsorption barrier of C_2H_2 is higher than that of H_2, the adsorption barrier of C_2H_2 is selected as E_R^{ad}. E_P^{de} is the energy difference between the transition state with the highest energy among all the hydrogenation reactions as well as the C_2H_4 desorption and the energy of the adsorbed C_2H_2 + 2H on the surface, as shown in Fig. 4. It should be mentioned that the coverage terms (θ_l and θ_*) have been expressed as energetic terms, and included in Eq. (9).

From Eq. (9), the overall reaction rate is mainly related to the E_R^{ad}, E_R^{de} and E_P^{de}, while the k_B, h and R are constants, T, P_R and P_P are the reaction conditions and ΔG is the intrinsic property of the reaction under the reaction conditions. Furthermore, the variable energetic terms, i.e., E_R^{ad}, E_R^{de} and E_P^{de}, are all in the exponential terms of the denominator and 0.1 eV difference between these energetic terms will result in a change of 30 times difference in the reaction rates at 350 K. Thus, some exponential terms in the denominator can be neglected if one energetic term is significant.

The energetic terms in the denominator of Eq. (9) are listed in Table 4. One can see from this table that E_P^{de} is the higher than $E_R^{ad} - E_R^{de} + E_P^{de}$ on Pd(111), Pd(100), Pd(211) and Pd(211)-defect surfaces. Therefore, E_P^{de} will be the effective barriers of acetylene hydrogenation on all the surfaces investigated in the current work. From Table 4, the activity for acetylene hydrogenation on Pd(111), Pd(211) and Pd(211)-defect are found to be similar while that on Pd(211) is slightly higher. Interestingly, Pd(100) shows the lowest activity and much lower than the other three surfaces investigated. The low activity of Pd(100) can be attributed to the fact that the adsorption of acetylene on Pd(100) is the strongest, leading to the low energy of the adsorbed C_2H_2 + 2H and hence the high effective desorption barrier of the product (i.e., high E_P^{de}), which is similar to the case of acetylene hydrogenation on Ni surfaces [71].

3.2. Influence of subsurface carbon on the activity and selectivity of ethylene formation on Pd

3.2.1. Adsorption of carbon at the surface and subsurface sites of Pd(111) and Pd(211)

The adsorption of one carbon atom was studied at the surface sites and the subsurface sites on both Pd(111) and Pd(211) surfaces, as well as the fourfold site (B5 site) on the Pd(211) surface. The adsorption energies of carbon atoms are listed in the Supporting information. On both surfaces the hcp sites are favored. In contrast, in the case of subsurface carbon, it is found that the octahedral sites are much favored on Pd(111) and the carbon atom binds strongest at the 4-fold on Pd(211), which is consistent with previous reported results [43,74].

In order to investigate further the coverage effects on the adsorption energies of the carbon atoms at different sites, the adsorption of the carbon atom at the favored surface and subsurface sites, *i.e.*, hcp and octahedral sites on Pd(111) and 4-fold sites on Pd(211), were studied by increasing the carbon coverage from 0.25 monolayer (ML) to 1 ML. The general trends of the adsorption energies of carbon per atom at different sites are shown in Fig. 5. It is obvious that the adsorption strength per atom becomes weaker with increasing coverage of carbon atoms due to the atom–atom repulsion. It is also found that the coverage of carbon atoms at the surface and subsurface sites influences the adsorption energies significantly while the adsorption energies of carbon atom(s) at the 4-fold sites of Pd(211) surface do not vary significantly with carbon coverage. These results are consistent with the work of Nørskov and co-workers [32].

The process of the carbon adsorption and the diffusion on Pd surfaces can be understood as follows. Since the step-edge sites are more active than the terrace sites for the C_2 species decomposition and the favored sites for the adsorption of carbon atoms are the 4-fold sites, this position is occupied first. With increasing coverage at these sites, some of the carbon atoms will diffuse to the subsurface sites of the terrace sites, since the subsurface sites of terrace are the second most favorable sites for carbon adsorption and the diffusion barrier is relatively small (0.10 eV from hcp and 0.11 eV from fcc) [74]. This continues to occur until the coverage at the subsurface sites reaches 0.25 ML. Since the adsorption energy of carbon atoms at the 4-fold sites is still negative when the coverage of carbon reaches 1 ML, we suggest that the 4-fold sites will be completely covered by carbon atoms. Because the adsorption energy of carbon is still slightly negative when the coverage of carbon atoms at the subsurface octahedral sites reaches 0.5 ML, this coverage can be considered to be thermodynamically favored. Therefore, the activity and selectivity were studied on Pd(111) with a coverage of subsurface carbon atoms up to 0.5 ML and on Pd(211) with the 4-fold sites completely covered by carbon atoms, denoted as Pd(111)–0.25C, Pd(111)–0.5C, and Pd(211)–C, respectively.

3.2.2. Acetylene hydrogenation on carbon-doped Pd surfaces

Pd(111) *surface* When the coverage of subsurface carbon is 0.25 ML, there are three types of adsorption sites, fcc sites with carbon atoms below (fcc-sub), fcc sites without carbon atoms below

Table 4
The exponential energetic terms in the denominator of Eq. (9). The definitions of these terms can be found in the main text and the caption of Fig. 4.

	$E_R^{ad} - E_R^{de} + E_P^{de}$ (eV)	E_P^{de} (eV)
Pd(111)	−0.49	1.07
Pd(100)	−0.84	1.34
Pd(211)	−0.83	0.97
Pd(211)-defect	−0.92	1.08

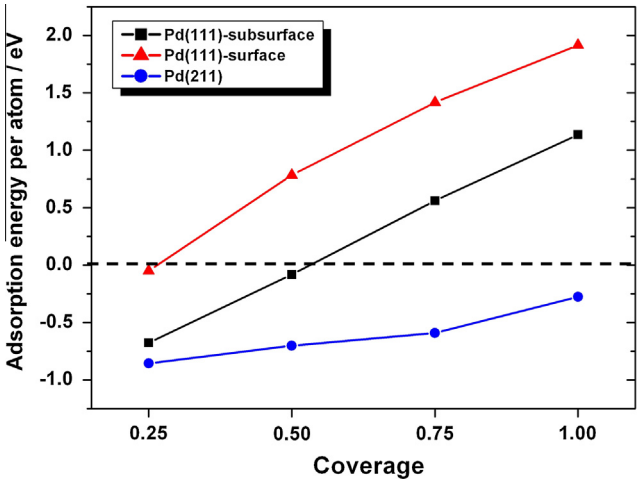

Fig. 5. Adsorption energies of carbon per atom at the surface sites and subsurface sites of Pd(111) surface and the 4-fold sites of Pd(211) surface. The energies are given with respect to the decomposition of gas-phase acetylene to adsorbed carbon and gas-phase H_2, according to the equation of ½ C_2H_2 → C + ½H_2.

(fcc), and hcp sites (hcp) and the relative adsorption energies of acetylene at these sites are listed in the Supporting information. It is obvious that the fcc sites without subsurface carbon atoms (fcc) are the favored sites. The reaction barriers were found to be 1.00 eV and 0.61 eV for the hydrogenation of C_2H_2 and C_2H_3, respectively.

When the coverage of subsurface carbon is 0.50 ML, four types of adsorption sites are present, fcc sites with carbon atoms below (fcc-sub), fcc sites without carbon atoms below (fcc), hcp sites in the carbon rows (hcp-in), and hcp sites between the carbon rows (hcp-between). The corresponding adsorption energies of C_2H_2 at these sites are summarized in the Supporting information. Obviously, the adsorption at the fcc sites is also the most stable on this surface. The hydrogenation barriers for C_2H_2 and C_2H_3 were found to be 0.91 eV and 0.48 eV, respectively, which are both lower than those over Pd(1 1 1)–0.25C.

Pd(2 1 1) *surface* On the carbon-doped surface, there are only two types of adsorption sites for acetylene, the 4-fold site under the step edges (B5 site) and the step edge site. The adsorption energies of both configurations are summarized in the Supporting information. It can be seen that the adsorption energy of C_2H_2 at the 4-fold sites of Pd(2 1 1)–C is only −0.15 eV (Fig. 6), which is much lower than that of clean Pd(2 1 1) surface, suggesting that the step-edge sites are the favored adsorption sites over the Pd(2 1 1)–C surface. In Fig. 6, we also present the adsorption configuration of C_2H_3 as well as the transition-state structures of C_2H_2 and C_2H_3 hydrogenation. The hydrogenation barriers of C_2H_2 and C_2H_3 hydrogenation were calculated to be 1.10 eV and 0.74 eV, respectively.

The energy profiles of the hydrogenation of acetylene, taking the adsorption and desorption processes into account, on the three surfaces, i.e., Pd(1 1 1)–0.25C, Pd(1 1 1)–0.5C and Pd(2 1 1)–C surfaces, are shown in Fig. 7. Using the method introduced above to measure the effective barriers on different Pd surfaces, we obtain the effective barriers for C_2H_2 hydrogenation to C_2H_4 over Pd(1 1 1)–0.25C, Pd(1 1 1)–0.5C, and Pd(2 1 1)–C to be 1.00 eV, 0.91 eV, and 1.10 eV, respectively. According to Eq. (2), the order of the activities over three surfaces should be Pd(1 1 1)–0.5C > Pd(1 1 1)–0.25C > Pd(2 1 1)–C.

3.2.3. Ethylene selectivity on carbon-doped Pd surfaces

When the subsurface carbon coverage is 0.25 ML, it is found that the 2-σ adsorption configuration (see Supporting information) is the most stable one among those possible adsorption geometries with an adsorption energy of −0.65 eV. When the subsurface carbon coverage is 0.5 ML, one can see that the most stable adsorption configuration is the π adsorption with an adsorption energy of −0.64 eV. At the step sites, the π adsorption is favored with an adsorption energy of −0.60 eV. Interestingly, the adsorption of C_2H_4 at those sites doped with carbon atoms are much weaker than those on clean Pd surfaces, which can be explained with the shift of the *d*-projected density of states of the surface Pd atoms to lower energy level, as shown in Fig. 8. The transition states (TSs) of C_2H_4 hydrogenation over Pd(1 1 1)–0.25C, Pd(1 1 1)–0.5C, and Pd(2 1 1)–C surfaces are presented in Supporting information. The hydrogenation barriers were calculated to be 0.98 eV, 0.91 eV, and 0.78 eV, respectively. Therefore, ΔE_a calculated with Eq. (2) on these surfaces are 0.33 eV, 0.27 eV, and 0.18 eV, respectively.

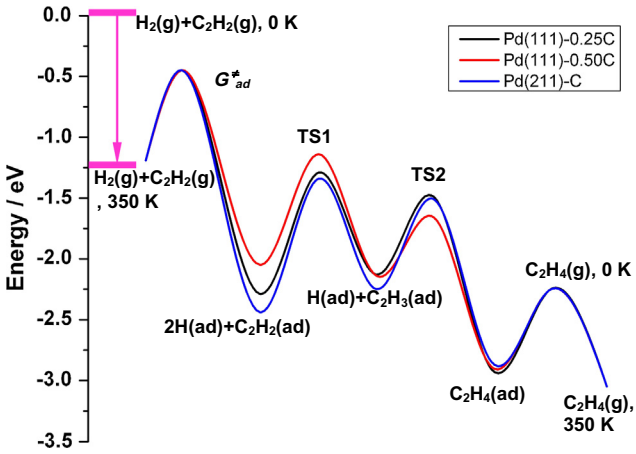

Fig. 7. Energy profiles of C_2H_2 hydrogenation on Pd(1 1 1)–0.25C, Pd(1 1 1)–0.5C, and Pd(2 1 1)–C surfaces under the standard pressure; the entropy effect is considered for the adsorption and desorption processes here. $G_{ad}^{\neq}$ is the transition-state energy of the adsorption of C_2H_2 on all the surfaces.

3.2.4. General discussion on the effect of subsurface carbon

Herein, the effect of the presence of subsurface carbon on Pd surfaces is addressed by comparing the effective barriers of acetylene hydrogenation on clean Pd (1 1 1) and Pd(2 1 1) surfaces with those on Pd(1 1 1)–0.25C, Pd(1 1 1)–0.5C, and Pd(2 1 1)–C surfaces. As described above, the effective barriers obtained on clean Pd(1 1 1) and Pd(2 1 1) are 1.07 eV and 0.97 eV, respectively, while those on Pd(1 1 1)–0.25C, Pd(1 1 1)–0.5C, and Pd(2 1 1)–C surfaces

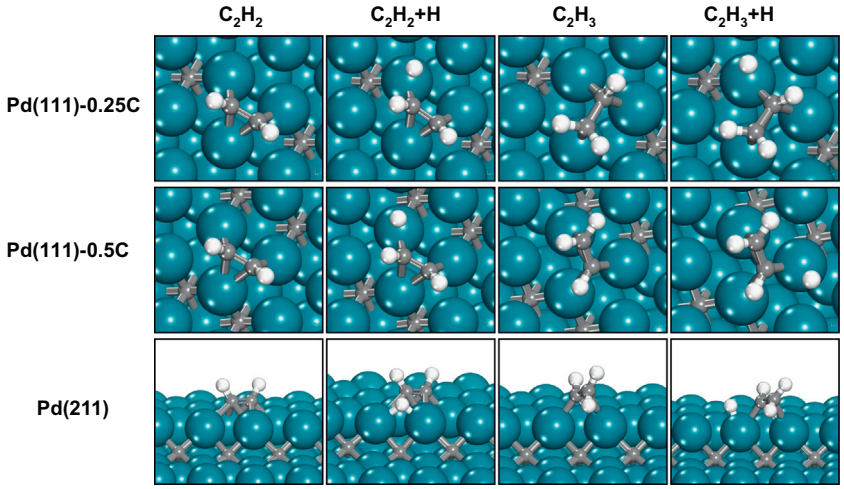

Fig. 6. Adsorption and hydrogenation transition-state structures of C_2H_2 and C_2H_3 on Pd(1 1 1)–0.25C, Pd(1 1 1)–0.5C and Pd(2 1 1)–C surfaces.

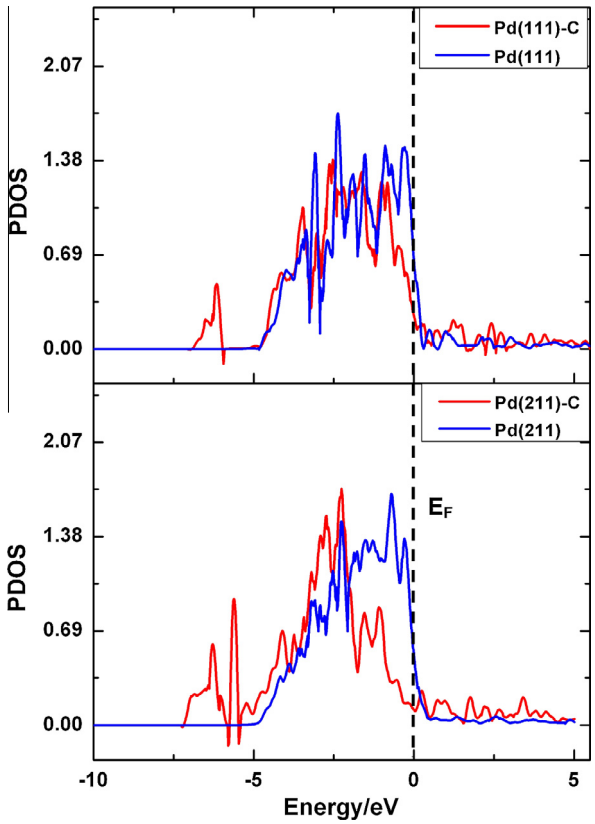

Fig. 8. *d*-Projected density of states (PDOS) of the Pd atoms in Pd(1 1 1), Pd(1 1 1)–0.25C, Pd(2 1 1), and Pd(2 1 1)–C. The Pd atoms projected are those that will bond with the reacting species. The Fermi level (E_f) has been set to be zero.

are 1.00 eV, 0.91 eV, and 1.10 eV, respectively. It is clear that the activity of Pd(1 1 1) slightly increases in the presence of subsurface carbon species, while that of Pd(2 1 1) slightly decreases. The activity of Pd(1 1 1) is lower than that on Pd(2 1 1), while the activity on Pd(1 1 1)–0.25C and Pd(1 1 1)–0.5C surfaces is higher than on Pd(2 1 1)–C surface at the reaction temperature. It should be noted that the previous experimental studies on the structure sensitivity of selective acetylene hydrogenation over the catalysts with shape-controlled Pd nanoparticles reported higher activity of the terrace sites than the step-edge sites by one order of magnitude [75]. Therefore, the activity of Pd(1 1 1) and Pd(2 1 1) surfaces with subsurface carbon species obtained from our calculations is in agreement with these results. This may also indicate that the Pd catalyst surface under real reaction condition might possess a Pd carbide structure. Furthermore, the selectivity of ethylene production on Pd surfaces is found to be increased in the presence of subsurface carbon species, which is consistent with the previously reported results [32].

3.3. Influence of subsurface hydrogen on the activity and selectivity of ethylene formation on Pd

Subsurface hydrogen has long been suggested to be active species in Pd-catalyzed hydrogenation of acetylene due to the ability of Pd to absorb hydrogen. In order to compare the hydrogenation ability of subsurface and surface hydrogen species and unravel the role subsurface hydrogen species playing in the selective hydrogenation of acetylene to produce ethylene, we studied the reaction process in the presence of subsurface hydrogen on Pd surfaces. Only the Pd(1 1 1) and Pd(2 1 1) surfaces are considered in this case and their surfaces with subsurface hydrogen atoms are denoted as Pd(1 1 1)/H_{sub} and Pd(2 1 1)/H_{sub}, respectively.

3.3.1. Acetylene hydrogenation on Pd(1 1 1) surface with subsurface hydrogen

The model used for the Pd(1 1 1)/H_{sub} surface was created by placing a hydrogen atom into every favorable subsurface site, tetrahedral sites in this work (see Supporting information) (the adsorption energy of hydrogen at this site is 0.06 eV per atom more stable than at the corresponding octahedral sites). Therefore, the Pd(1 1 1) surface with 1 ML of hydrogen atoms at the subsurface tetrahedral sites (see Supporting information) was employed to study the hydrogenation reactions with the subsurface and surface hydrogen atoms.

Our previous work, investigating the physical origin of the high reactivity of subsurface hydrogen in catalytic hydrogenation of CH_3 on Ni(1 1 1) surfaces [76], reported that the hydrogenation by diffused hydrogen from the subsurface sites has relatively lower barriers, which is consistent with the work of Sautet and co-workers [77]. Therefore, the process of the diffusion of subsurface hydrogen atoms to the surface sites followed by the hydrogenation of the C_2 species, i.e., C_2H_2, C_2H_3 and C_2H_4, was investigated in the current work.

Acetylene is found to adsorb at the fcc site, under which there is no hydrogen atom adsorbed, of Pd(1 1 1)/H_{sub} surface, as shown in Fig. 9. One can see that there are three possibilities for the hydrogenation of acetylene with the subsurface hydrogen atoms, which are marked in Fig. 9. All three pathways were studied and the energy profiles are shown in Fig. 10, as well as the TS structures of the hydrogen attacking. One can see that pathway 2 should be the favored one among the three pathways and the effective barrier is 0.43 eV and the reaction energy, ($E_{FS} - E_{IS}$) in Fig. 10, is −0.14 eV.

The vinyl group (C_2H_3) formed is found to adsorb at the bridge sites on Pd(1 1 1)/H_{sub} surface. There are six possible hydrogenation pathways of C_2H_3 on the surface by five subsurface hydrogen atoms, which are marked in Fig. 9, due to the asymmetric adsorption structure of it. The energy profiles of the six pathways are shown in Fig. 10. The favored pathway shown in Fig. 10 for the hydrogenation of C_2H_3 is pathway 3, with an effective barrier of 0.24 eV and reaction energy of −0.96 eV. With the calculated values of the reaction barriers and reaction energies, we can obtain the energy profile of the hydrogenation of acetylene with subsurface hydrogen atoms (shown in Fig. 12), which, therefore, can be utilized to estimate the activity of this process by measuring the effective barriers.

In order to obtain the selectivity for ethylene formation from the hydrogenation of acetylene with the subsurface hydrogen, we also calculated the adsorption energy and hydrogenation barrier of ethylene on Pd(1 1 1)/H_{sub} surface. The adsorption geometry of ethylene is shown in Supporting information, and the energy profile of ethylene hydrogenation by the subsurface hydrogen is shown in Fig. 10 with the TS structures. It should be mentioned that the favored adsorption configuration of ethylene is changed from di-σ-bonded on clean Pd(1 1 1) to π-bonded on Pd(1 1 1)/H_{sub}, which is consistent with the experimental results reported before [78]. The adsorption energy was calculated to be −0.64 eV, and the effect hydrogenation barrier is 0.64 eV, indicating that ΔE_a will be 0 eV, according to Eq. (2).

Comparison can be made between the hydrogenation of adsorbed C_2 species by the subsurface hydrogen and the surface bound hydrogen atoms: We calculated the energies of the TSs of C_2H_2, C_2H_3, and C_2H_4 hydrogenation with the surface hydrogen atoms, the structures of which are shown in Supporting information. The reaction barriers were calculated to be 0.73 eV, 0.42 eV, and 0.80 eV for the corresponding hydrogenation of C_2H_2, C_2H_3,

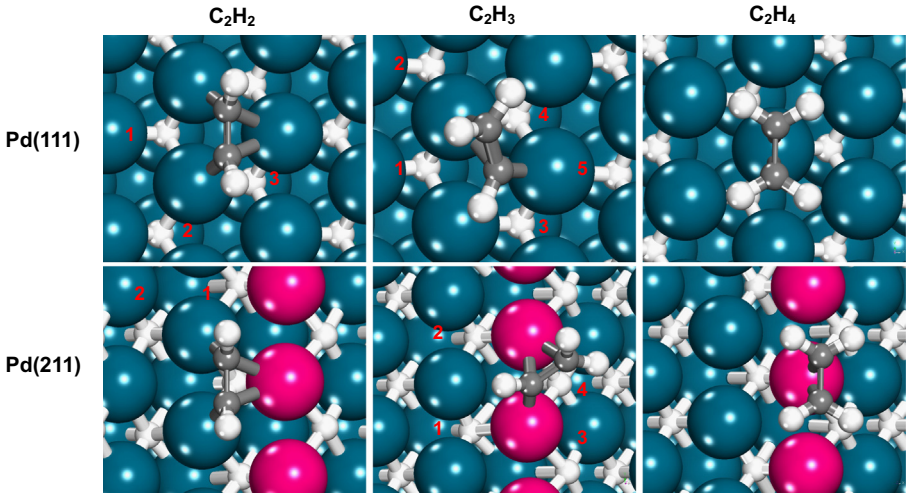

Fig. 9. Adsorption structures of C_2H_2, C_2H_3, and C_2H_4 hydrogenation on Pd(1 1 1) and Pd(2 1 1) surfaces with subsurface hydrogen.

and C_2H_4. The energy profile of acetylene hydrogenation is shown in Fig. 12. ΔE_a was calculated to be 0.16 eV.

3.3.2. Acetylene hydrogenation on Pd(2 1 1) with subsurface hydrogen

The Pd(2 1 1)/H_{sub} surface was modeled by placing a hydrogen atom into every subsurface octahedral site, as well as the fourfold sites, since we find that the favored subsurface site is the octahedral site on Pd(2 1 1) surface, which is different to that found on Pd(1 1 1). This difference may be attributed to the repulsion between the hydrogen atoms adsorbed at the fourfold sites and those at the subsurface tetrahedral sites at the step edge.

The favored adsorption geometry of acetylene on Pd(2 1 1)/H_{sub} surface is shown in Fig. 9. There are two possibilities for the acetylene hydrogenation by the subsurface hydrogen atoms, which are marked as 1 and 2 in Fig. 9. The energy profiles of corresponding hydrogenation pathways are shown in Fig. 11 with the TS structures (TS2). It is found that the favored pathway should be the hydrogenation with the subsurface hydrogen marked as 1. The effective barrier of this process was calculated to be 0.44 eV, and the reaction energy is −0.40 eV.

The vinyl group is also found to adsorb at the bridge sites of the step edge of the Pd(2 1 1)/H_{sub} surface. As shown in Fig. 9, there are six possible hydrogenation pathways of C_2H_3 on the surface by five subsurface hydrogen atoms, which is similar to the case of vinyl hydrogenation on Pd(1 1 1)/H_{sub} surface. Among the six pathways, two of them include the diffusion of subsurface hydrogen to the surface followed by the reaction with hydrogen while the other four pathways show the direct hydrogenation of the substrate by the hydrogen atoms adsorbed at the fourfold sites. The energy profiles of all the six pathways are shown in Fig. 11. The favored pathway is found to be pathway 5, which shows the hydrogenation of C_2H_3 by the hydrogen atom adsorbed at the fourfold site to produce ethylene. The energy profile of the whole pathway is also obtained and shown in Fig. 12.

The adsorption energy of ethylene on the Pd(2 1 1)/H_{sub} surface was obtained to be −0.83 eV. The hydrogenation of ethylene takes place via two pathways, one being the ethylene hydrogenation by the diffused hydrogen atoms from the subsurface site and the other being the direct hydrogenation by the hydrogen atom at the fourfold site, as shown in Fig. 11. The hydrogenation barrier was calculated to be 0.68 eV. Therefore, we can obtain ΔE_a on this surface to be −0.15 eV.

The corresponding hydrogenation barriers of C_2H_2, C_2H_3, and C_2H_4 by the surface bound hydrogen atoms on the Pd(2 1 1)/H_{sub} surface were calculated to be 0.77 eV, 0.46 eV and 0.70 eV, respectively. The TS structures are shown in Supporting information, and the energy profile is shown in Fig. 12. ΔE_a for the determination of the selectivity of ethylene formation is −0.13 eV.

3.3.3. General discussion on the effect of subsurface hydrogen

The effective barriers determined for the hydrogenation of acetylene by the subsurface hydrogen on Pd(1 1 1) and Pd(2 1 1) are 0.43 eV and 0.44 eV, respectively, while those for the hydrogenation by surface bound hydrogen are 0.73 eV and 0.77 eV, respectively, indicating that the subsurface hydrogen atoms are more active than the surface bound ones on Pd-hydride surfaces. Considering that the effective barriers of acetylene hydrogenation on clean Pd(1 1 1) and Pd(2 1 1) surfaces are 1.07 eV and 0.97 eV, respectively, and those on Pd(1 1 1)–0.25C, Pd(1 1 1)–0.5C and Pd(2 1 1)–C surfaces are 1.00 eV, 0.91 eV and 1.10 eV, respectively, one can see that the activity on Pd surfaces with subsurface hydrogen atoms are much higher than either clean Pd surfaces or Pd surfaces with subsurface carbon species, which is consistent with the previous experimental and theoretical results [31,34,44,79,80].

ΔE_a on Pd(1 1 1)/H_{sub} surface for acetylene hydrogenation by subsurface and surface bound hydrogen atoms are 0 eV and 0.16 eV, respectively, and those on Pd(2 1 1) surface by subsurface hydrogen are −0.15 eV and −0.13 eV, respectively. Compared with those results obtained on clean Pd(1 1 1) and Pd(2 1 1) surfaces being 0.06 eV and −0.3 eV, respectively, and those on Pd(1 1 1)–0.25C, Pd(1 1 1)–0.5C and Pd(2 1 1)–C being 0.38 eV, 0.27 eV and 0.18 eV, respectively, one can see that the selectivities on Pd surfaces with subsurface hydrogen are all much lower than those on Pd surfaces with subsurface carbon species, and are marginally higher than clean Pd surfaces. However, considering our results in Section 3.2 showing that the dominant Pd surfaces under real reaction conditions might be Pd carbide-like structures, it may be more meaningful to compare the results on Pd surfaces with subsurface hydrogen with those obtained on Pd surfaces with subsurface carbon species. Therefore, it is clear that the selectivity for ethylene formation is lowered in the presence of subsurface hydrogen on Pd surfaces, which is also consistent with the previous reported results [31,32,34,44,79].

3.4. Selectivity of ethylene formation on the alloyed flat and stepped surfaces

Many experimental results showed an enhancement of the selectivity for C_2H_4 formation when 1B metals are added to Pd catalysts for C_2H_2 hydrogenation. In order to understand the effect of

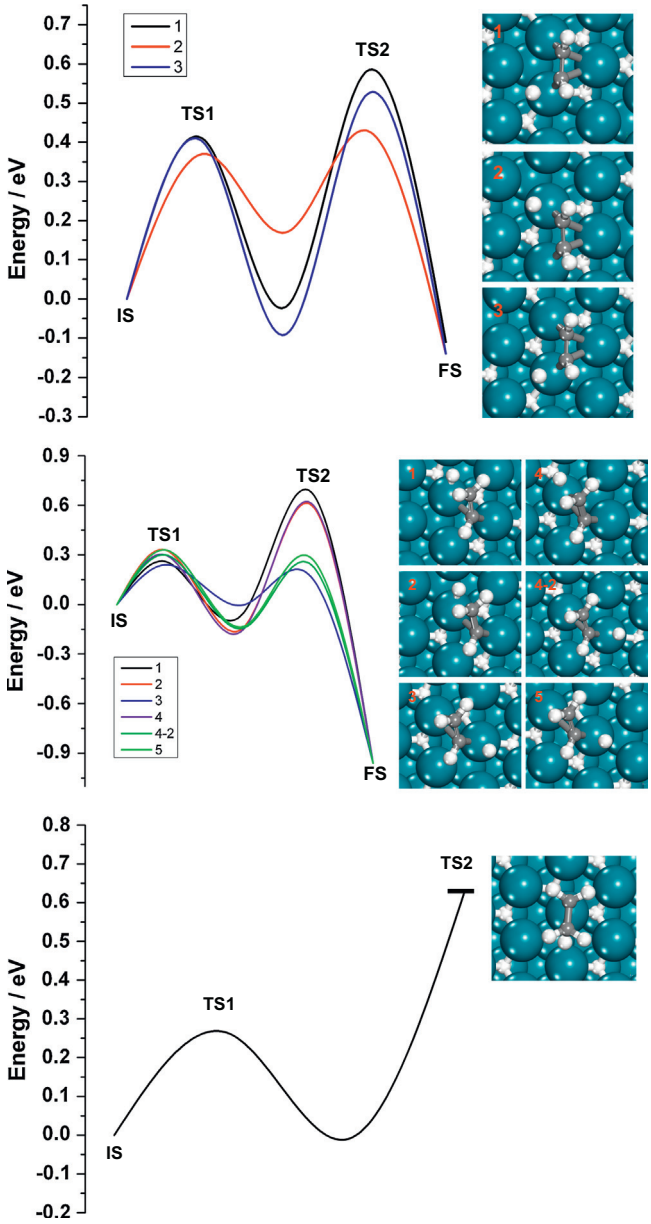

Fig. 10. Energy profiles of the hydrogenation of C_2H_2, C_2H_3, and C_2H_4 by subsurface hydrogen on Pd(1 1 1) surface with subsurface hydrogen. IS, TS1, TS2, and FS are the adsorption states of C_2 species, transition states of the subsurface hydrogen diffusion to the surface, transition states of the C_2 species hydrogenation by the diffused surface hydrogen atoms and the adsorption states of the product, respectively. Also shown are the corresponding TS2 structures.

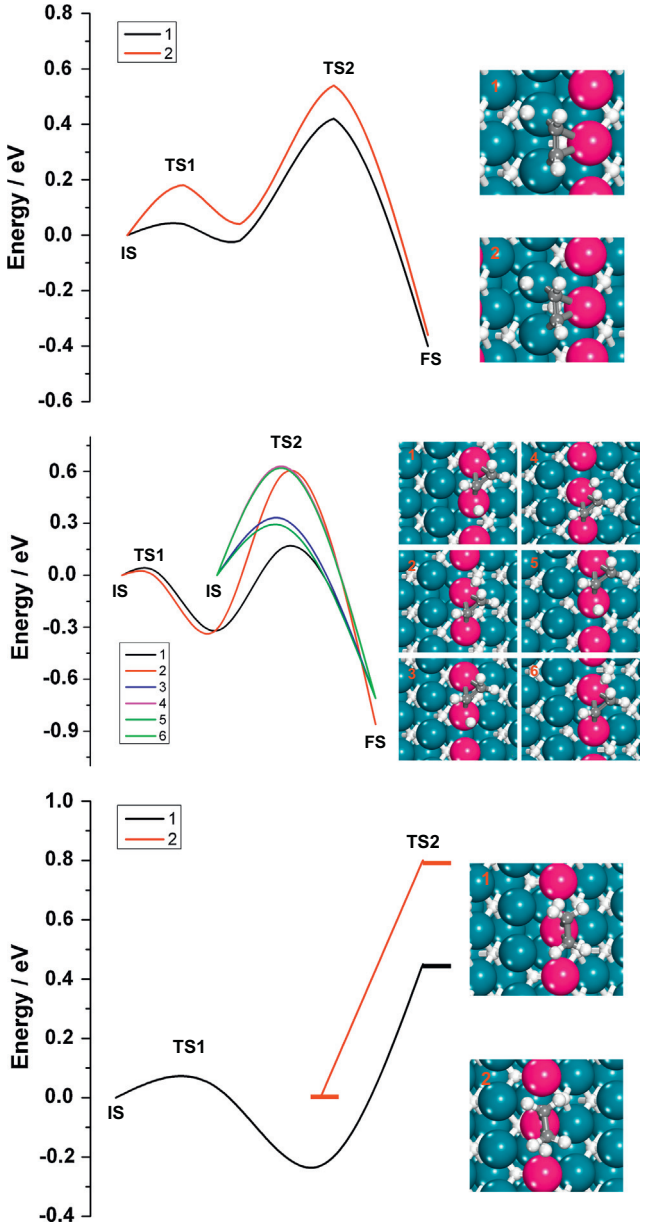

Fig. 11. Energy profiles of the hydrogenation of C_2H_2, C_2H_3, and C_2H_4 by subsurface hydrogen on Pd(2 1 1) surface with subsurface hydrogen. IS, TS1, TS2, and FS have the same definition with those in Fig. 10. The TS2 structures are also shown here.

the promoter on the selectivity, the adsorption and hydrogenation of C_2H_4 on Pd–M (M = Cu, Ag, and Au) surface alloys as a function of the surface composition were examined.

3.4.1. Pd–M/Pd(1 1 1) surface alloys

The adsorption energies and the hydrogenation barriers of C_2H_4 are listed in Table 5 as well as the C–H distances at the TSs as a function of the surface concentration of Cu, Ag, and Au. One can see that the adsorption energies of ethylene on Pd–Cu/Pd(1 1 1) surface at all Cu coverages from 0.25 ML to 0.75 ML are all close to that on pure Pd(1 1 1), indicating that Cu has a minor influence on the adsorption energy of ethylene on Pd(1 1 1). This is consistent with previously reported results [55]. However, all other surfaces studied using Cu, Ag, and Au alloyed with Pd(1 1 1) result in lower adsorption energies compared with that found on pure Pd(1 1 1). Since C_2H_4 adsorbs on the Pd sites on all Pd–M/Pd(1 1 1) (M = Cu, Ag, Au) surfaces (Fig. 13), the geometric effect can be largely ruled out, and the decreases in C_2H_4 adsorption energies on Pd–M/Pd(1 1 1) compared with those on Pd(1 1 1) indicate that the electronic effect plays an important role in reducing the adsorption energies. Fig. 13 illustrates the adsorption structures of C_2H_4 on Pd–M/Pd(1 1 1) surface alloys with the surface Pd/M ratios ranging from 3:1, 1:1, and 1:3 (Pd/M) to a complete overlayer of the M metal on the surface of the Pd. As shown in Fig. 13, C_2H_4 does not adsorb on Pd–Ag/Pd(1 1 1) and Pd–Au/Pd(1 1 1) surfaces when a complete monolayer of Ag and Au is present and hence hydrogenation is unlikely to occur on these surfaces. The geometries of the

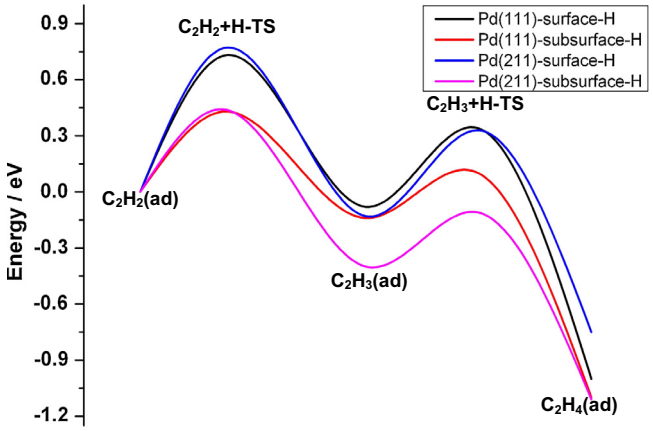

Fig. 12. Energy profiles of the hydrogenation of C_2H_2 to produce C_2H_4 by the surface bound and subsurface hydrogen atoms on Pd(1 1 1) and Pd(2 1 1) surfaces with subsurface hydrogen atoms.

transition states of C_2H_4 hydrogenation on Pd–M/Pd(1 1 1) for the surface compositions of 3:1, 1:1, and 1:3 (Pd/M) are shown in Fig. 14 for M = Cu, Ag, and Au.

These data and structures can be summarized as follows. Firstly, the adsorption energies of C_2H_4 on Pd–Ag/Pd(1 1 1) and Pd–Au/Pd(1 1 1) decrease with the increasing coverage of surface Ag and Au atoms while those on Pd–Cu/Pd(1 1 1) do not show a large variation until the coverage of Cu on the surface increases to 1 ML. Secondly, the reaction barriers of C_2H_4 hydrogenation decrease with the coverage of surface Cu, Ag, and Au atoms albeit a relatively small change on Cu-doped systems at coverages from 0.5 ML to 1 ML. The C–H distances at the TSs of different doped metals with the same coverage were found to be very similar. Thirdly, C_2H_4 adsorbs on the alloyed surface with a di-σ structure on Pd atoms when the surface is Pd rich. However, on becoming dopant rich, the adsorption of C_2H_4 changes to a π adsorption configuration on all three alloyed surfaces. This π adsorption geometry was also observed on the overlayer of Cu on Pd(1 1 1). Finally, at the transition states, the reacting hydrogen atoms are located on the same metal atoms as the carbon atoms with which it reacts. This is in agreement with previous theoretical results of hydrogenation reactions [35,69,81–85]. More importantly, ethylene adsorbs on the alloyed surfaces with a π-bonded structure at all the transition states.

The influence of subsurface carbon/hydrogen was also considered for the modified systems, and the adsorption energies for hydrogen and carbon are listed in the Supporting information (Table S3). Importantly, we found that the subsurface species were only stable at low surface coverages of the modifier and were less stable compared to the alloyed surfaces than on Pd(1 1 1) itself. Therefore, it is unlikely that the formation of carbide or hydride has a significant influence on the surface reaction in the modified systems, and their effect was not considered in any of the studies reported, herein.

3.4.2. Pd–M/Pd(2 1 1) surface alloys

For comparison, the effect of Cu, Ag, and Au on the stepped Pd surface (Pd(2 1 1)) was also examined. The coverage effect of these metals was not studied in this work; instead, an extreme model in which the step-edge Pd atoms are replaced by M (M = Cu, Ag, and Au) effectively blocking the step sites of the Pd(2 1 1) surface was used in this study. This model was utilized as the concentration of the defect sites is relatively low on the catalyst surface, and previous work has clearly shown that the dopant metals like Ag may decorate the low coordination sites due to the inertness of these metals [86]. Therefore, it is likely for all of the defect sites to be decorated when these metals are doped. Table 6 lists the adsorption energies and the hydrogenation barriers of C_2H_4 on Pd–M/Pd(2 1 1) (M = Cu, Ag, and Au) surfaces together with the C–H distances at the TSs. Fig. 15 shows the adsorption geometries of C_2H_4 and the transition-state structures in C_2H_4 hydrogenation on Pd–M/Pd(2 1 1). From these data, it is clear that the adsorption energies of C_2H_4 on Pd–Ag/Pd(2 1 1) and Pd–Au/Pd(2 1 1) are very similar but is doubled on Pd–Cu/Pd(2 1 1). However, the addition of the second metal significantly reduces the C_2H_4 adsorption energy compared with that on the pure Pd(2 1 1) surface. Secondly, all the hydrogenation barriers of C_2H_4 were found to be similar with the lowest barrier on Pd–Au/Pd(2 1 1). Thirdly, although the C–H distances at the TSs are similar on Pd–Ag/Pd(2 1 1) and Pd–Au/Pd(2 1 1), a decrease in the distance was found on Pd–Cu/Pd(2 1 1) surface. Finally, the π adsorption geometry for C_2H_4 is favored in all three cases.

3.4.3. General discussion on the effects of surface alloys on the selectivity

To understand the origin of alloying effects of Cu, Ag and Au on the C_2H_4 selectivity on Pd-based catalysts for C_2H_2 hydrogenation reaction, the difference (ΔE_a) between the hydrogenation barriers and the desorption barriers (approximated by the adsorption energies) of C_2H_4 on Pd–M/Pd(1 1 1) and Pd–M/Pd(2 1 1) (M = Cu, Ag, and Au) surfaces was compared. The variation in ΔE_a with the metal dopants and their surface coverage is shown in Fig. 16 and Table S4. It should be noted that, as no adsorption occurred on either the full overlayer of Ag or Au on Pd(1 1 1), no comparison is possible with the Cu/Pd(1 1 1) (full overlayer of Cu on Pd(1 1 1)).

Table 5
Adsorption energies (E_{ad}) of ethylene, reaction barriers (E_a) of ethylene hydrogenation, and the C–H distances at the TSs on Pd–M/Pd(1 1 1) (M = Cu, Ag, and Au) surface alloys with different coverage of M.

	Coverage (ML)	E_{ad} (eV)	E_a (eV)	Distance (Å)
Pd–Cu/Pd(1 1 1)	0.25	−0.85	0.92	1.47
	0.50	−0.86	0.78	1.42
	0.75	−0.82	0.80	1.46
	1.00	−0.37	0.79	1.53
Pd–Ag/Pd(1 1 1)	0.25	−0.75	0.91	1.48
	0.50	−0.66	0.77	1.44
	0.75	−0.54	0.72	1.54
	1.00	−0.05	–	–
Pd–Au/Pd(1 1 1)	0.25	−0.71	0.88	1.50
	0.50	−0.56	0.60	1.48
	0.75	−0.45	0.55	1.52
	1.00	−0.06	–	–

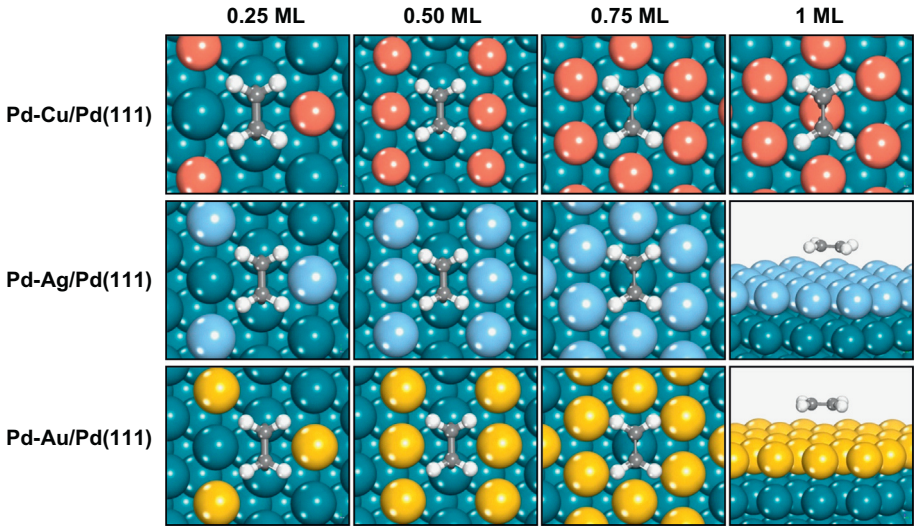

Fig. 13. Adsorption structures of C_2H_4 on Pd–Cu/Pd(1 1 1), Pd–Ag/Pd(1 1 1), and Pd–Au/Pd(1 1 1) surfaces. The red, light blue, and yellow balls denote copper, silver, and gold, respectively. This notation is used throughout this paper. (For interpretation of the references to color in this figure legend, the reader is referred to the web version of this article.)

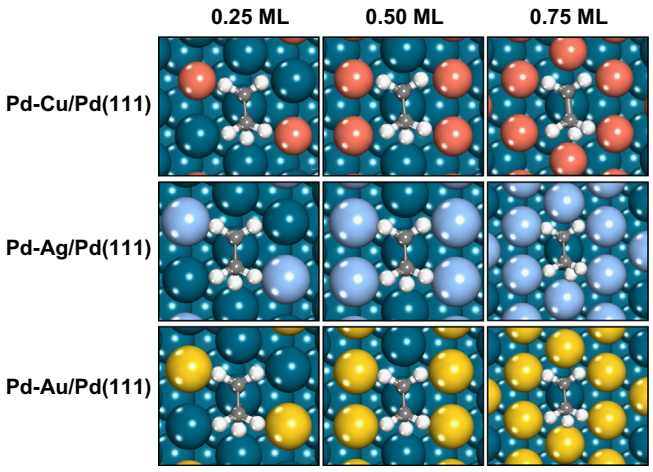

Fig. 14. Transition-state structures of C_2H_4 hydrogenation on Pd–Cu/Pd(1 1 1), Pd–Ag/Pd(1 1 1), and Pd–Au/Pd(1 1 1) surfaces.

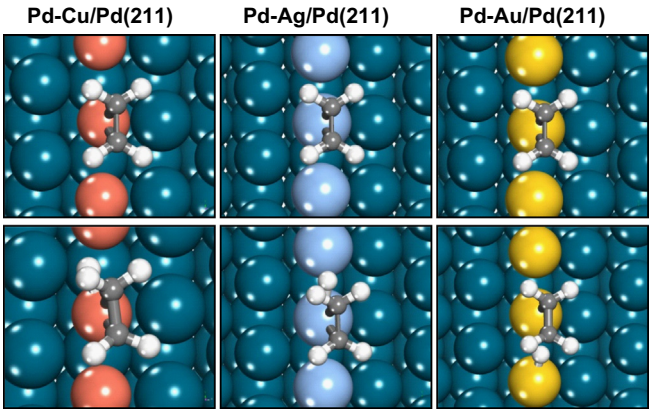

Fig. 15. Adsorption structures (above panel) of C_2H_4 and transition-state structures (below panel) of C_2H_4 hydrogenation on Pd–Cu/Pd(2 1 1), Pd–Ag/Pd(2 1 1), and Pd–Au/Pd(2 1 1) surfaces.

Table 6
Adsorption energies (E_{ad}) of ethylene, reaction barriers (E_a) of ethylene hydrogenation, and the C–H distances at the TSs on Pd–M/Pd(2 1 1) (M = Cu, Ag, and Au) surface alloys. Also listed are the calculated values of ΔE_a.

	Pd–Cu/Pd(2 1 1)	Pd–Ag/Pd(2 1 1)	Pd–Au/Pd(2 1 1)
E_{ad} (eV)	−0.72	−0.35	−0.39
E_a (eV)	0.98	1.00	0.88
Distance (Å)	1.46	1.59	1.58
ΔE_a (eV)	0.26	0.65	0.49

On the alloyed (1 1 1) surfaces, the Cu-doped Pd(1 1 1) surfaces show lower values of ΔE_a compared with Ag- and Au-alloyed systems (Fig. 16), indicating that the selectivity of C_2H_4 is the lowest on Cu-modified Pd surfaces. Moreover, all the Ag and Au systems show a positive value of ΔE_a, indicating a positive effect on the selectivity, with Cu this is only true when the system has a surface coverage of 3:1 (Pd/Cu). At 1:1 and 1:3, ΔE_a become negative, indicating that the over-hydrogenation reaction might be favored. When the comparison is made regarding the Ag- and Au-doped systems, we found that the general trend of the selectivity from pure Pd(1 1 1) to the 0.75 ML Ag coverage is increasing, while the selectivity of 0.25 ML Au coverage possesses the highest selectivity among the clean Pd(1 1 1) and Au-doped surfaces.

To quantitatively address the determining factor for the difference of ΔE_a on different surfaces, a new energy decomposition method is used here (see Scheme 1). From our previous work, the reaction barriers can be decomposed into three terms: the two energy costs for the two reactants to move from the initial state (IS), usually the adsorption state (ad), to the transition state (TS) without the other reactant, and the interaction energy (E_{int}) between two reactants at the TS [69,87,88]. From the definition in Eq. (2):

$$\begin{aligned}\Delta E_a &= E_{a,hydr} - |E_{ad}| \\ &= (E_{C_2H_4,TS} - E_{C_2H_4,ad}) + (E_{H,TS} - E_{H,ad}) + E_{int} - |E_{ad,C_2H_4}| \end{aligned} \quad (10)$$

where $E_{C_2H_4,TS}$ and $E_{H,TS}$ are the energies of C_2H_4 and H at the transition state, respectively, $E_{C_2H_4,ad}$ and $E_{H,ad}$ are the energies of C_2H_4 and

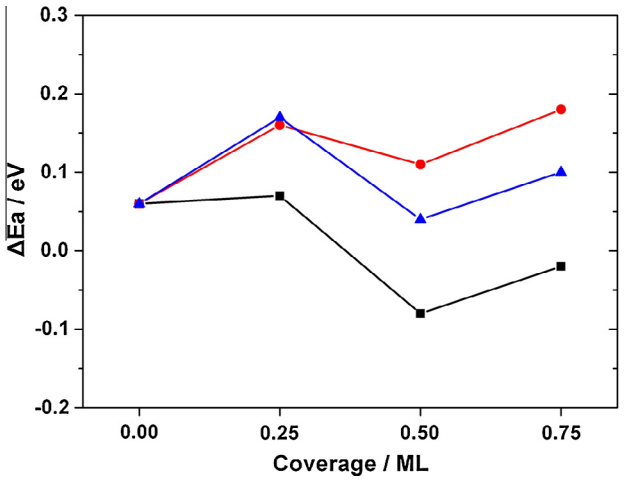

Fig. 16. The trend of ΔE_a changes with the coverage of Cu, Ag, and Au on Pd–Cu/Pd(1 1 1) (black squares and line), Pd–Ag/Pd(1 1 1) (red circles and line) and Pd–Au/Pd(1 1 1) (blue triangles and line) surfaces. The unit of the coverage is monolayer (ML). (For interpretation of the references to color in this figure legend, the reader is referred to the web version of this article.)

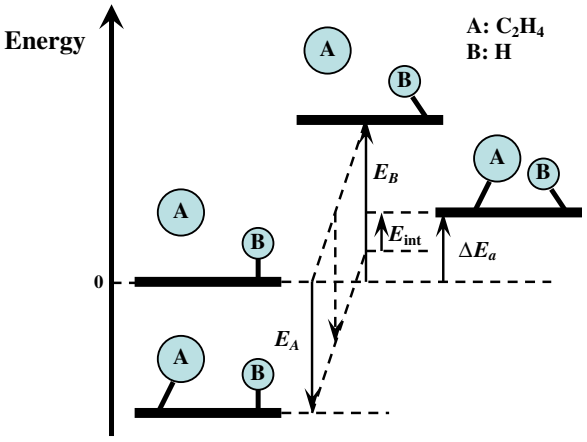

Scheme 1. Schematic diagram of ΔE_a decomposition. According to this scheme, ΔE_a is decomposed into three terms: E_A is the energy for reactant A to move from the gas phase to the transition state (TS) without reactant B. E_B is the energy for reactant B to move from the adsorption state to the transition state (TS) without reactant A. E_{int} is a measure of the interaction energy between A and B at the TS. The energy of A in gas phase and B at the adsorption state is set as zero point.

H at the initial state, respectively, E_{int} is the interaction energy between C_2H_4 and H at the transition state. As the adsorption energies of C_2H_4 in the present work are all negative:

$$\begin{aligned}\Delta E_a &= (E_{C_2H_4,TS} - E_{C_2H_4,ad}) + (E_{H,TS} - E_{H,ad}) + E_{int} + E_{ad,C_2H_4} \\ &= (E_{C_2H_4,TS} - E_{C_2H_4,ad}) + (E_{H,TS} - E_{H,ad}) + E_{int} + E_{C_2H_4,ad} \\ &\quad - E_{C_2H_4} - E_{slab} \\ &= (E_{C_2H_4,TS} - E_{C_2H_4} - E_{slab}) + (E_{H,TS} - E_{H,ad}) + E_{int} \qquad (11)\end{aligned}$$

If we define $E_A = E_{C_2H_4,TS} - E_{C_2H_4} - E_{slab}$ and $E_B = E_{H,TS} - E_{H,ad}$, then ΔE_a can be decomposed into three terms, which are E_A, E_B and E_{int}, as shown in Scheme 1. In fact, one can find that E_A can also be defined as the adsorption energy of C_2H_4 at the transition state, according to the definition of adsorption energies in Eq. (1). The relative values of E_A, E_B, E_{int}, and ΔE_a are listed in Table S4.

From the results listed in Tables S4 and 6, one can obtain the following conclusions regarding the effect of Cu, Ag, and Au on the ethylene selectivity on Pd(1 1 1) and Pd(2 1 1):

1. The general trend of ΔE_a on Cu- and Au-doped Pd(1 1 1) is similar to that of E_B, indicating that the energy costs for hydrogen from the adsorption states to the transition states play an important role in the selectivity on these surfaces.
2. The general trend of ΔE_a on Ag-doped Pd(1 1 1) is found to be similar to that of E_A, which should be the adsorption energy of C_2H_4 at the transition state.
3. On the alloyed (2 1 1) surfaces, it is clear that all the dopants increase the value of ΔE_a and thus enhance the selectivity of C_2H_4. In this case, the alloying of the (2 1 1) surface results in the surface switching from over-hydrogenation (Pd(2 1 1)) to selective hydrogenation of acetylene to ethylene. The deactivation of the Pd step edge using the Cu, Ag, and Au is suggested to be the origin of the large increases in the selectivity observed on modifying the catalyst experimentally.

4. Conclusions

In this work, extensive DFT calculations were carried out to estimate the activity and selectivity of acetylene hydrogenation to ethylene with several models in order to unravel the underlying influences of surface structures, subsurface species (carbon and hydrogen), and surface alloys on the activity and selectivity. The activity was measured by calculating the reaction rates of acetylene hydrogenation to produce ethylene with a general two-step model previously proposed by our group. The selectivity of ethylene was measured by comparing the energy differences between the hydrogenation barriers and the absolute values of ethylene adsorption energies, which is one of the first attempts to quantitatively compare different selectivity of this process. The following conclusions are obtained:

1. The activity of different surface sites for acetylene hydrogenation follows the order of Pd(2 1 1) > Pd(1 1 1) ≈ Pd(2 1 1)-defect ≫ Pd(1 0 0), indicating that it is the specific arrangement of atoms rather than the coordination number that determines the activity. The low activity of Pd(1 0 0) surface may be explained by the strong adsorption of acetylene on the surface.
2. Over clean Pd, more open surfaces result in over-hydrogenation to form ethane with the close-packed Pd(1 1 1) surface being the most selective system.
3. In the presence of subsurface species (carbon and hydrogen), the activity and the selectivity will be varied. The activity of the flat surface is found to increase in the presence of subsurface carbon atoms, while the activity of the step surface decreases, which is consistent with the experimental results.
4. In the presence of subsurface hydrogen species, we found that the activity of acetylene hydrogenation, either with subsurface hydrogen or surface bound hydrogen, is higher than those on clean Pd surfaces and Pd surfaces with subsurface carbon. The selectivity is found to be lower than Pd–C surfaces.
5. On alloying with Cu, Ag and Au, the selectivity of (1 1 1) surfaces for the hydrogenation of acetylene to ethylene is enhanced with the exception of Cu-rich surfaces. The reasons for this are also analyzed in detail and addressed in this work.
6. Further increases in the selectivity are observed on alloying the (2 1 1) surfaces. In these cases, blocking the low coordination sites at the step edge results in significant increases in the hydrogenation selectivity with respect to ethylene formation over the production of ethane.

This work provides an understanding of the influence of the surface structures and surface alloys on both the activity and selectivity from the molecular level, which may provide some design criteria for similar systems in heterogeneous catalysis.

Acknowledgments

This work is financially supported by EPSRC and Johnson Matthey through the CASTech program. The authors would like to thank The Queen's University of Belfast for computing time. B.Y. also acknowledges the financial support of Dorothy Hodgkin Postgraduate Award (DHPA) studentship jointly funded by EPSRC and Johnson Matthey.

Appendix A. Supplementary material

Supplementary data associated with this article can be found, in the online version, at http://dx.doi.org/10.1016/j.jcat.2013.05.027.

References

[1] A. Borodziński, G.C. Bond, Catal. Rev. – Sci. Eng. 48 (2006) 91–144.
[2] A. Borodziński, G.C. Bond, Catal. Rev. – Sci. Eng. 50 (2008) 379–469.
[3] S. Asplund, J. Catal. 158 (1996) 267–278.
[4] I.Y. Ahn, J.H. Lee, S.S. Kum, S.H. Moon, Catal. Today 123 (2007) 151–157.
[5] I.Y. Ahn, J.H. Lee, S.K. Kim, S.H. Moon, Appl. Catal. A – Gen. 360 (2009) 38–42.
[6] N. López, B. Bridier, J. Pérez-Ramírez, J. Phys. Chem. C 112 (2008) 9346–9350.
[7] P. Praserthdam, S. Phatanasri, J. Meksikarin, Catal. Today 63 (2000) 209–213.
[8] B. Ngamsom, N. Bogdanchikova, M.A. Borja, P. Praserthdam, Catal. Commun. 5 (2004) 243–248.
[9] Q.W. Zhang, J. Li, X.X. Liu, Q.M. Zhu, Appl. Catal. A – Gen. 197 (2000) 221–228.
[10] N.A. Khan, S. Shaikhutdinov, H.J. Freund, Catal. Lett. 108 (2006) 159–164.
[11] W. Huang, J.R. McCormick, R.F. Lobo, J.G. Chen, J. Catal. 246 (2007) 40–51.
[12] A. Sárkány, A. Horváth, A. Beck, Appl. Catal. A – Gen. 229 (2002) 117–125.
[13] L. Guczi, Z. Schay, G. Stefler, L.F. Liotta, G. Deganello, A.M. Venezia, J. Catal. 182 (1999) 456–462.
[14] J. Osswald, R. Giedigkeit, R.E. Jentoft, M. Armbrüster, F. Girgsdies, K. Kovnir, T. Ressler, Y. Grin, R. Schlögl, J. Catal. 258 (2008) 210–218.
[15] J. Osswald, K. Kovnir, M. Armbrüster, R. Giedigleit, R.E. Jentoft, U. Wild, Y. Grin, R. Schlögl, J. Catal. 258 (2008) 219–227.
[16] K. Kovnir, J. Osswald, M. Armbrüster, D. Teschner, G. Weinberg, U. Wild, A. Knop-Gericke, T. Ressler, Y. Grin, R. Schlögl, J. Catal. 264 (2009) 93–103.
[17] M. Armbrüster, K. Kovnir, M. Behrens, D. Teschner, Y. Grin, R. Schlögl, J. Am. Chem. Soc. 132 (2010) 14745–14747.
[18] J.A. Anderson, J. Mellor, R.P.K. Wells, J. Catal. 261 (2009) 208–216.
[19] M.W. Tew, H. Emerich, J.A. van Bokhoven, J. Phys. Chem. C 115 (2011) 8457–8465.
[20] S. Bailey, R.L.C. Bonne, J.S. Booth, C. Griffiths, M.J. Watson, in: WO/2004/108638 (Ed.), Selective Hydrogenation Process and Catalyst Therefor, 2004.
[21] W. Huang, W. Pyrz, R.F. Lobo, J.G.G. Chen, Appl. Catal. A – Gen. 333 (2007) 254–263.
[22] W.J. Kim, J.H. Kang, I.Y. Ahn, S.H. Moon, Appl. Catal. A – Gen. 268 (2004) 77–82.
[23] J.H. Kang, E.W. Shin, W.J. Kim, J.D. Park, S.H. Moon, Catal. Today 63 (2000) 183–188.
[24] J.H. Kang, E.W. Shin, W.J. Kim, J.D. Park, S.H. Moon, J. Catal. 208 (2002) 310–320.
[25] W.J. Kim, J.H. Kang, I.Y. Ahn, S.H. Moon, J. Catal. 226 (2004) 226–229.
[26] I.Y. Ahn, W.J. Kim, S.H. Moon, Appl. Catal. A – Gen. 308 (2006) 75–81.
[27] E.W. Shin, J.H. Kang, W.J. Kim, J.D. Park, S.H. Moon, Appl. Catal. A – Gen. 223 (2002) 161–172.
[28] F. Studt, F. Abild-Pedersen, T. Bligaard, R.Z. Sørensen, C.H. Christensen, J.K. Nørskov, Science 320 (2008) 1320–1322.
[29] B. Bridier, J. Pérez-Ramírez, J. Am. Chem. Soc. 132 (2010) 4321–4327.
[30] S. Abelló, D. Verboekend, B. Bridier, J. Pérez-Ramírez, J. Catal. 259 (2008) 85–95.
[31] D. Teschner, J. Borsodi, A. Wootsch, Z. Révay, M. Hävecker, A. Knop-Gericke, S.D. Jackson, R. Schlögl, Science 320 (2008) 86–89.
[32] F. Studt, F. Abild-Pedersen, T. Bligaard, R.Z. Sørensen, C.H. Christensen, J.K. Nørskov, Angew. Chem. – Int. Ed. 47 (2008) 9299–9302.
[33] K.M. Neyman, S. Schauermann, Angew. Chem. – Int. Ed. 49 (2010) 4743–4746.
[34] M. García-Mota, B. Bridier, J. Pérez-Ramírez, N. López, J. Catal. 273 (2010) 92–102.
[35] P.A. Sheth, M. Neurock, C.M. Smith, J. Phys. Chem. B 107 (2003) 2009–2017.
[36] D.H. Mei, P.A. Sheth, M. Neurock, C.M. Smith, J. Catal. 242 (2006) 1–15.
[37] D.H. Mei, M. Neurock, C.M. Smith, J. Catal. 268 (2009) 181–195.
[38] P.A. Sheth, M. Neurock, C.M. Smith, J. Phys. Chem. B 109 (2005) 12449–12466.
[39] J. Andersin, N. López, K. Honkala, J. Phys. Chem. C 113 (2009) 8278–8286.
[40] S. González, K.M. Neyman, S. Shaikhutdinov, H.J. Freund, F. Illas, J. Phys. Chem. C 111 (2007) 6852–6856.
[41] P. Sautet, F. Cinquini, ChemCatChem 2 (2010) 636–639.
[42] I.V. Yudanov, K.M. Neyman, N. Rösch, Phys. Chem. Chem. Phys. 6 (2004) 116–123.
[43] S.M. Kozlov, I.V. Yudanov, H.A. Aleksandrov, N. Rösch, Phys. Chem. Chem. Phys. 11 (2009) 10955–10963.
[44] D. Teschner, Z. Revay, J. Borsodi, M. Hävecker, A. Knop-Gericke, R. Schlögl, D. Milroy, S.D. Jackson, D. Torres, P. Sautet, Angew. Chem. – Int. Ed. 47 (2008) 9274–9278.
[45] G. Kresse, J. Hafner, Phys. Rev. B 47 (1993) 558–561.
[46] G. Kresse, J. Hafner, Phys. Rev. B 49 (1994) 14251–14269.
[47] G. Kresse, J. Furthmuller, Comput. Mater. Sci. 6 (1996) 15–50.
[48] G. Kresse, J. Furthmuller, Phys. Rev. B 54 (1996) 11169–11186.
[49] J.P. Perdew, Y. Wang, Phys. Rev. B 45 (1992) 13244–13249.
[50] P.E. Blöchl, Phys. Rev. B 50 (1994) 17953–17979.
[51] G. Kresse, D. Joubert, Phys. Rev. B 59 (1999) 1758–1775.
[52] A. Alavi, P. Hu, T. Deutsch, P.L. Silvestrelli, J. Hutter, Phys. Rev. Lett. 80 (1998) 3650–3653.
[53] Z.P. Liu, P. Hu, J. Am. Chem. Soc. 125 (2003) 1958–1967.
[54] A. Michaelides, Z.P. Liu, C.J. Zhang, A. Alavi, D.A. King, P. Hu, J. Am. Chem. Soc. 125 (2003) 3704–3705.
[55] N. López, C. Vargas-Fuentes, Chem. Commun. 48 (2012) 1379–1391.
[56] J.D. Cox, D.D. Wagman, V.A. Medvedev, CODATA Key Values for Thermodynamics., Hemisphere, New York, 1989.
[57] L.V. Gurvich, I.V. Veyts, C.B. Alcock, Thermodynamic Properties of Individual Substances, fourth ed., Hemisphere, New York, 1989.
[58] J.W. Medlin, M.D. Allendorf, J. Phys. Chem. B 107 (2003) 217–223.
[59] F. Mittendorfer, C. Thomazeau, P. Raybaud, H. Toulhoat, J. Phys. Chem. B 107 (2003) 12287–12295.
[60] P.G. Belelli, R.M. Ferullo, N.J. Castellani, Surf. Sci. 604 (2010) 386–395.
[61] B. Bridier, N. López, J. Pérez-Ramírez, Dalton Trans. 39 (2010) 8412–8419.
[62] J.C. Dunphy, M. Rose, S. Behler, D.F. Ogletree, M. Salmeron, P. Sautet, Phys. Rev. B 57 (1998) R12705–R12708.
[63] L.V. Moskaleva, H.A. Aleksandrov, D. Basaran, Z.J. Zhao, N. Rösch, J. Phys. Chem. C 113 (2009) 15373–15379.
[64] L.V. Moskaleva, Z.X. Chen, H.A. Aleksandrov, A.B. Mohammed, Q. Sun, N. Rösch, J. Phys. Chem. C 113 (2009) 2512–2520.
[65] Z.X. Chen, H.A. Aleksandrov, D. Basaran, N. Rösch, J. Phys. Chem. C 114 (2010) 17683–17692.
[66] D. Basaran, H.A. Aleksandrov, Z.X. Chen, Z.J. Zhao, N. Rösch, J. Mol. Catal. A – Chem. 344 (2011) 37–46.
[67] J. Andersin, K. Honkala, Surf. Sci. 604 (2010) 762–769.
[68] X.-M. Cao, R. Burch, C. Hardacre, P. Hu, Catal. Today 165 (2011) 71–79.
[69] B. Yang, D. Wang, X.-Q. Gong, P. Hu, Phys. Chem. Chem. Phys. 13 (2011) 21146–21152.
[70] B. Yang, X.-M. Cao, X.-Q. Gong, P. Hu, Phys. Chem. Chem. Phys. 14 (2012) 3741–3745.
[71] B. Yang, R. Burch, C. Hardacre, G. Headdock, P. Hu, ACS Catal. 2 (2012) 1027–1032.
[72] J. Cheng, P. Hu, P. Ellis, S. French, G. Kelly, C.M. Lok, J. Phys. Chem. C 112 (2008) 1308–1311.
[73] J. Cheng, P. Hu, Angew. Chem. – Int. Ed. 50 (2012) 7650–7654.
[74] L. Nykanen, J. Andersin, K. Honkala, Phys. Rev. B 81 (2010) 10.
[75] A.E. Yarulin, R.M. Crespo-Quesada, E.V. Egorova, L.L.K. Minsker, Kinet. Catal. 53 (2012) 253–261.
[76] A. Michaelides, P. Hu, A. Alavi, J. Chem. Phys. 111 (1999) 1343–1345.
[77] V. Ledentu, W. Dong, P. Sautet, J. Am. Chem. Soc. 122 (2000) 1796–1801.
[78] D. Stacchiola, W.T. Tysoe, Surf. Sci. 540 (2003) L600–L604.
[79] D. Teschner, J. Borsodi, Z. Kis, L. Szentmiklosi, Z. Revay, A. Knop-Gericke, R. Schlogl, D. Torres, P. Sautet, J. Phys. Chem. C 114 (2010) 2293–2299.
[80] P. Tiruppathi, J.J. Low, A.S.Y. Chan, S.R. Bare, R.J. Meyer, Catal. Today 165 (2011) 106–111.
[81] P. Crawford, P. Hu, J. Chem. Phys. 124 (2006) 044705.
[82] J. Cheng, P. Hu, P. Ellis, S. French, G. Kelly, C.M. Lok, J. Phys. Chem. C 112 (2008) 9464–9473.
[83] J. Cheng, T. Song, P. Hu, C.M. Lok, P. Ellis, S. French, J. Catal. 255 (2008) 20–28.
[84] J. Cheng, P. Hu, P. Ellis, S. French, G. Kelly, C.M. Lok, J. Phys. Chem. C 114 (2010) 1085–1093.
[85] X.Q. Gong, R. Raval, P. Hu, J. Chem. Phys. 122 (2005) 024711.
[86] R.T. Vang, K. Honkala, S. Dahl, E.K. Vestergaard, J. Schnadt, E. Laegsgaard, B.S. Clausen, J.K. Nørskov, F. Besenbacher, Nat. Mater. 4 (2005) 160–162.
[87] Z.P. Liu, P. Hu, J. Chem. Phys. 114 (2001) 8244–8247.
[88] Z.P. Liu, P. Hu, J. Chem. Phys. 115 (2001) 4977–4980.